INVITED PAPER *Special Section on Distinguished Papers in Photonics*

Growth Mechanism of Polar-Plane-Free Faceted InGaN Quantum Wells*

Yoshinobu MATSUDA[†a)], **Mitsuru FUNATO**[†], *Nonmembers*, *and* **Yoichi KAWAKAMI**[†b)], *Member*

SUMMARY   The growth mechanisms of three-dimensionally (3D) faceted InGaN quantum wells (QWs) on $(\bar{1}\bar{1}2\bar{2})$ GaN substrates are discussed. The structure is composed of $(\bar{1}\bar{1}2\bar{2})$, $\{\bar{1}10\bar{1}\}$, and $\{\bar{1}100\}$ planes, and the cross sectional shape is similar to that of 3D QWs on (0001). However, the 3D QWs on $(\bar{1}\bar{1}2\bar{2})$ and (0001) show quite different inter-facet variation of In compositions. To clarify this observation, the local thicknesses of constituent InN and GaN on the 3D GaN are fitted with a formula derived from the diffusion equation. It is suggested that the difference in the In incorporation efficiency of each crystallographic plane strongly affects the surface In adatom migration.
key words: Ⅲ*-nitride semiconductor, three-dimensional structure, polychromatic emission*

1. Introduction

Semiconductor microstructures are expected to play an important role in the next generation light emitters. For example, three-dimensionally (3D) faceted InGaN quantum wells (QWs) have received increasing attention due to the following reasons. The In composition and InGaN thickness are facet-dependent, which results in the polychromatic emission, including white [1]–[6]. Furthermore, the emission spectra can be tuned via structure control [2], and the 3D structure can enhance the light extraction efficiency [6]. These characteristics may lead to the efficient emission of arbitrary spectra without phosphors. Toward this goal, it is indispensable to identify the crystal growth mechanisms in 3D faceted QWs.

Figure 1 shows schematics of 3D InGaN QWs on (a) (0001) and (b) $(\bar{1}\bar{1}2\bar{2})$, and (c) their typical luminescence spectra. To date, 3D QWs are usually fabricated on the (0001) plane [1]–[6], and are composed of, for example, (0001), $\{11\bar{2}2\}$. and $\{11\bar{2}0\}$ facets [Fig. 1 (a)]. The emission wavelengths vary in the order of top (0001) > inclined $\{11\bar{2}2\}$ > side $\{11\bar{2}0\}$ mainly due to the In spatial distribution. One remarkable feature of this type of 3D QWs is that the efficiency of the longest wavelength emission tends to be low because the polar (0001) plane, where the optical transition probability is low due to the strain-induced piezoelectric fields [7], [8], is responsible for the longest wavelength emission. On the other hand, the recently developed 3D QWs on $(\bar{1}\bar{1}2\bar{2})$ are composed of $(\bar{1}\bar{1}2\bar{2})$, $\{\bar{1}10\bar{1}\}$, and $\{\bar{1}100\}$
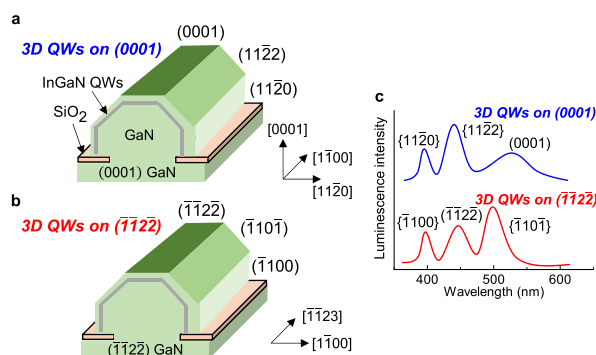
Fig. 1   Schematics of 3D QWs on (a) (0001) and (b) $(\bar{1}\bar{1}2\bar{2})$, and (c) their typical luminescence spectra.

facets, exclusive of the polar (0001) plane [Fig. 1 (b)] [9]. As expected, it has experimentally been demonstrated that all the facet QWs exhibit quite short radiative lifetimes.

For the 3D QWs on (0001), the aforementioned facet-dependence of the emission wavelength (i.e. In composition) has been attributed to active In adatom migration from the inclined $\{11\bar{2}2\}$ to top (0001) facets [10]. In contrast, the emission wavelengths from the 3D QWs on $(\bar{1}\bar{1}2\bar{2})$ are in the order of inclined $\{\bar{1}10\bar{1}\}$ > top $(\bar{1}\bar{1}2\bar{2})$ > side $\{\bar{1}100\}$ [9]. Because both 3D QWs have similar trapezoidal cross sections, the observed difference indicates the presence of an unknown factor in addition to adatom migration. In this study, we discuss the growth mechanism that determines the inter-facet variation of the emission properties, comparing the 3D QWs on $(\bar{1}\bar{1}2\bar{2})$ with those on (0001). We demonstrate that the In incorporation efficiency into each facet plays an important role.

2. Experimental Procedures

The 3D QWs on $(\bar{1}\bar{1}2\bar{2})$ and the reference 3D QWs on (0001) were created on SiO$_2$-mask-patterned $(\bar{1}\bar{1}2\bar{2})$ and (0001) GaN, respectively, by metalorganic vapor phase epitaxy. The corresponding details of the growth conditions were described in Refs. [2] and [9]. The QW local structural properties were assessed by scanning electron microscopy (SEM), transmission electron microscopy (TEM), and energy dispersive X-ray spectroscopy (EDS). The experimental results were analyzed using the diffusion equation with consideration of the In incorporation efficiency.

3. QW Local Structural Properties

Figure 2 shows cross-sectional SEM images and local QW structural properties of the 3D QW on (0001) [(a) and (b)] and ($\bar{1}\bar{1}2\bar{2}$) [(c) and (d)]. In Figs. 2 (b) and 2 (d), open triangles are effective GaN and InN widths derived from the local InGaN thickness and In composition. It should be noted that the well width and In composition in Fig. 2 (b) were estimated by SEM and EDS equipped to the SEM; for this purpose, InGaN thick films and InGaN/GaN 200 period superlattices were grown on the 3D GaN structures because of the experimental resolution lager than the dimensions of QWs. On the other hand, those in Fig. 2 (d) were estimated by TEM and EDS equipped to the TEM. We confirmed that both SEM + EDS and TEM + EDS provide essentially the same results. Here, the top (0001) and ($\bar{1}\bar{1}2\bar{2}$) facets in Figs. 2 (a) and 2 (c) are flat and concave down, respectively. The origins of this difference are under investigation, and the differenece in the surface diffusion of adatoms between the inclined and top facets would be one of the plausible factors.

Generally, the inter-facet emission-wavelength distributions can be accounted for by the local In composition and well width. For the 3D QWs on (0001) [Figs. 2 (a) and 2 (b)], the top (0001) facet QW has the widest well thickness and the highest In composition, resulting in the longest wavelength emission [Fig. 1 (c)]. For the 3D QWs on ($\bar{1}\bar{1}2\bar{2}$), the well thickness distribution is similar to that of the 3D QWs on (0001). However, the QW with the highest In composition is formed on the inclined ($\bar{1}10\bar{1}$) facet, and the In composition ($\sim$23%) is much higher than that ($\sim$15%) of the top ($\bar{1}\bar{1}2\bar{2}$) facet. As a result, the longest-wavelength emission relies on the inclined {$\bar{1}10\bar{1}$} facet, which is also supported by the transition energy calculations [9].

To further discuss the inter-facet variation of In compositions, the effective GaN and InN thickness distributions in Figs. 2 (b) and 2 (d) are compared. In general, a film thickness d should be proportional to a growth rate v. Moreover, the growth rate can be approximated as $v \propto kJ$, where k and

J are incorporation efficiency and the sum of fluxes of atoms from the gas phase and adatoms migrating on the surface, respectively. Thus, higher k and/or J result in a thicker film. For the 3D QWs on (0001) [Fig. 2 (b)], GaN and InN thicknesses increase from the inclined ($11\bar{2}2$) to the top (0001) facets. This was attributed to the active Ga and In adatom migration from the inclined ($11\bar{2}2$) to the top (0001) facets. Furthermore, more active In adatom migration, which can read from the thickness ratio between the (0001) and ($11\bar{2}2$) facets, leads to the In-rich QWs on the top (0001) facet. That is, the GaN and InN thicknesses in the 3D QWs on (0001) are chiefly determined by the mass transport (J). Meanwhile, for the 3D QWs on ($\bar{1}\bar{1}2\bar{2}$) [Fig. 2 (d)], the GaN thickness distribution exhibits a trend similar to that of the 3D QWs on (0001), which means that the GaN thickness also depends on the mass transport. However, the InN thickness slightly decreases from the inclined ($\bar{1}10\bar{1}$) to the top ($\bar{1}\bar{1}2\bar{2}$) facets, which suggests that the InN thickness in the 3D QWs on ($\bar{1}\bar{1}2\bar{2}$) depends not only on the mass transport (J) but also on the facet-dependent In incorporation efficiency (k).

Multiple papers reported In compositions of InGaN QWs grown on differently oriented substrates [11]–[13]. Our experiments showed that In compositions of the (0001), $\pm$($11\bar{2}2$), and $\pm$($1\bar{1}01$) planar QWs under the same growth condition as the 3D QWs are as follows: 26.9% for ($\bar{1}10\bar{1}$) > 23.6% for ($1\bar{1}01$) > 18.4% for ($11\bar{2}2$) > 10.8% for ($\bar{1}\bar{1}2\bar{2}$) > 8.9% for (0001) [9]. For the 3D QWs on (0001), the top (0001) facet QWs have a higher In composition than the inclined ($11\bar{2}2$) facet QWs, in spite of the lower In incorporation efficiency. This observation is consistent with the active In adatom migration from the inclined ($11\bar{2}2$) to the top (0001) facets, which suggests that the higher In incorporation efficiency of the ($11\bar{2}2$) plane is hindered by such active In adatom migration. On the other hand, the In compositions of the ($\bar{1}\bar{1}2\bar{2}$) and ($\bar{1}10\bar{1}$) facet QWs in the 3D QWs on ($\bar{1}\bar{1}2\bar{2}$) have a tendency similar to those of each planar QWs. Here, it should be noted that the ($\bar{1}10\bar{1}$) plane shows a significantly higher In composition, which is presumed to promote efficient incorporation of In adatoms and suppress the In adatom migration to the top ($\bar{1}\bar{1}2\bar{2}$) facet. As a result, the InN thickness of the inclined ($\bar{1}10\bar{1}$) facet becomes slightly thicker than that of the top ($\bar{1}\bar{1}2\bar{2}$) facet [Fig. 2 (d)].

4. Diffusion Equation Analyses

To support the above assertion, diffusion equation analyses were performed. Figure 3 (a) shows a cross-sectional SEM image and the definitions of the coordinates. The 3D structure was grown on a mask pattern with a larger window width than that in Fig. 2 (c) to appropriately estimate the adatom diffusion length on the top ($\bar{1}\bar{1}2\bar{2}$) facet. The local InGaN thickness and In compositions were estimated by SEM and EDS equipped to the SEM in the same manner as Fig. 2 (b). The estimated local thickness of GaN and InN on both ($\bar{1}\bar{1}2\bar{2}$) and ($\bar{1}10\bar{1}$) facets were plotted in Figs. 3 (b) and 3 (c), respectively. These thickness distributions were fitted based on the diffusion equation. The detailed analysis pro-

Fig. 2 Cross-sectional SEM images and QW local structural properties of the 3D QW on (0001) [(a) and (b)] and ($\bar{1}\bar{1}2\bar{2}$) [(c) and (d)], respectively.
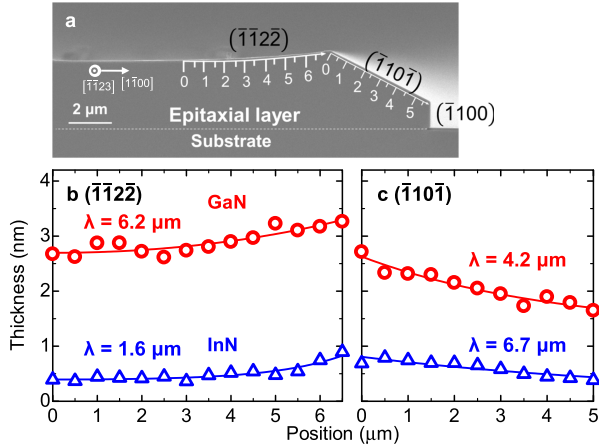
Fig. 3 (a) Cross-sectional SEM image. Local GaN and InN thicknesses on (b) $(\bar{1}\bar{1}2\bar{2})$ and (c) $(\bar{1}10\bar{1})$ facets at positions designated in (a).

Fig. 4 A model to simulate the growth dynamics on the 3D structure. The fluxes of atoms from the gas phase and adatoms migrating on the surface are indicated by the black and colored allows, respectively.

cedure can be found in Ref. [10]. For Ga, the estimated surface diffusion lengths, $\lambda_{Ga}^{(\bar{1}\bar{1}2\bar{2})}$ and $\lambda_{Ga}^{(\bar{1}10\bar{1})}$, are 6.2 and 4.2 μm, respectively. For In, $\lambda_{In}^{(\bar{1}\bar{1}2\bar{2})}$ and $\lambda_{In}^{(\bar{1}10\bar{1})}$ are 1.6 and 6.7 μm, respectively.

Note that higher growth temperatures generally shorten diffusion lengths by promoting evaporation, while activating migration. Therefore, a shorter diffusion length suggests more active migration. For the 3D QWs on (0001), the Ga diffusion length on the top (0001) facet was 5.2 μm, while that on the inclined (11$\bar{2}$2) facet was 3.1 μm [10]. This trend is quite similar to the present observation, which suggests that Ga adatoms behave similarly on both the 3D QWs. On the other hand, the In diffusion lengths show the opposite tendency between the 3D QWs on (0001) and $(\bar{1}\bar{1}2\bar{2})$; on (0001), those were 2.7 μm on the top facet and 1.6 μm on the inclined facet [10], which suggests more drastic migration on the inclined {11$\bar{2}$2} facets. Such active In adatom migration overcomes the higher In incorporation efficiency of the (11$\bar{2}$2) plane, resulting in a lower In composition. On the other hand, for the 3D QWs on $(\bar{1}\bar{1}2\bar{2})$, the much longer In diffusion length on the inclined $(\bar{1}10\bar{1})$ than that on the top $(\bar{1}\bar{1}2\bar{2})$ means passive In adatom migration on the inclined {$\bar{1}10\bar{1}$} facets most likely due to the higher In incorporation efficiency. These findings are consistent with the above-mentioned assertion.

Inter-facet variation of the In composition affected by In incorporation efficiencies is also found in Ref. [5]. The inversed pyramids composed of closely neighboring {1$\bar{1}$01} and {11$\bar{2}$2} facet QWs provide facet-dependent polychromatic emission; the emission wavelength of the {1$\bar{1}$01} facet QWs is 20 nm longer than the {11$\bar{2}$2} facet QWs. This tendency can be explained by a similar scenario based on the higher In incorporation efficiency of the (1$\bar{1}$01) plane.

5. A Model Calculation of Mass Transport under the Influence of In Incorporation

In this section, we propose a simple model based on the one-

dimensional inter-facet surface migration. In this model, the flux of adatoms migrating from the inclined to top facet J_m is assumed to be influenced by the atom incorporation efficiency into the solid phase. The atom incorporation efficiency of each crystallographic plane is described in Sect. 3.
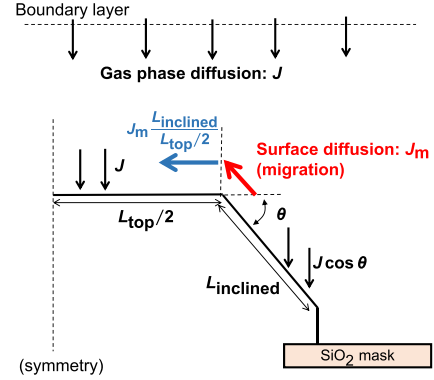
Figure 4 schematically shows this model, where parameters on the top and inclined planes are represented as subscripts, while those on the planar and facet QWs are designated by superscripts. From the relationship $d \propto v \propto kJ$, we obtain

$$\frac{J_{top}^{facet}}{J_{inclined}^{facet}} = \frac{d_{top}^{facet}/k_{top}}{d_{inclined}^{facet}/k_{inclined}}. \quad (1)$$

The incorporation ratio, $k_{top}/k_{inclined}$, is equal to the film thickness ratio of planar QWs grown along the corresponding directions under the same condition, that is, $d_{top}^{planar}/d_{inclined}^{planar}$, because J is common for the planar QWs irrespective of the crystallographic orientations. Then, we have

$$\frac{J_{top}^{facet}}{J_{inclined}^{facet}} = \frac{d_{top}^{facet}/d_{top}^{planar}}{d_{inclined}^{facet}/d_{inclined}^{planar}}. \quad (2)$$

On the inclined facet, the flux from the gas phase becomes $J \cos\theta$ due to the geometrical configuration, where θ is the angle between the top and inclined facets. In addition, adatoms are assumed to migrate from the inclined to top facet with a flux of J_m. Thus, the total flux on the inclined facet is expressed as $J \cos\theta - J_m$. Noting that J_m (as well as J) is defined as an area density, the flux into the top facet can be expressed as $J + J_m \frac{L_{inclined}}{L_{top}/2}$, where L_{top} and $L_{inclined}$ are the facet widths of the 3D structures. Therefore, we obtain

$$\frac{J + J_m \frac{L_{inclined}}{L_{top}/2}}{J \cos\theta - J_m} = \frac{d_{top}^{facet}/d_{top}^{planar}}{d_{inclined}^{facet}/d_{inclined}^{planar}}. \quad (3)$$

The assumptions in this model are as follows: (1) only the half of the top facet (width of $L_{top}/2$) is considered due to the structural symmetry, (2) J_m is constant on the entire area of the inclined facet, and (3) adatom diffusion to/from the

Table 1 Effective GaN and InN thickness of the top and inclined facets in the 3D QWs on (0001) and $(\bar{1}\bar{1}2\bar{2})$. Those are the avaraged values of the plots for the each facet in Figs. 2 (b) and 2 (d).

3D QWs	Plane	GaN (nm)	InN (nm)
on (0001)	Top (0001)	4.09	0.68
	Inclined $(11\bar{2}2)$	1.45	0.13
on $(\bar{1}\bar{1}2\bar{2})$	Top $(\bar{1}\bar{1}2\bar{2})$	2.90	0.50
	Inclined $(\bar{1}10\bar{1})$	2.08	0.60

side facet can be ignored due to the small area.

For the planar QWs, we have experimentally determined the thickness ratios as $d^{\mathrm{planar}}_{(0001)}/d^{\mathrm{planar}}_{(11\bar{2}2)} = 1.02$ and 0.44 for GaN and InN, respectively, and similarly, $d^{\mathrm{planar}}_{(\bar{1}\bar{1}2\bar{2})}/d^{\mathrm{planar}}_{(\bar{1}10\bar{1})}$ is 1.75 for GaN and 0.58 for InN [9]. For the 3D structures, the thicknesses were evaluated from Figs. 2 (b) and 2 (d), as summarized in Table 1. Using these values with Eq. (3), the normalized flux J_{m}/J is calculated to be +0.09 for GaN and +0.37 for InN in the 3D QWs on (0001), which means that surface In adatoms more drastically migrate from the inclined to top facets than Ga adatoms. On the other hand, for the 3D QWs on $(\bar{1}\bar{1}2\bar{2})$, J_{m}/J is -0.09 for GaN and +0.08 for InN. It is noteworthy that J_{m}/J for InN in the 3D QWs on $(\bar{1}\bar{1}2\bar{2})$ is much smaller than that in 3D QWs on (0001), which indicates that less In adatoms migrate from the inclined to top facets. This trend well agrees with the above discussion. Although the surface diffusion direction of Ga adatoms in the 3D QWs on $(\bar{1}\bar{1}2\bar{2})$ is inconsistent with the diffusion equation analyses, J_{m}/J for GaN is relatively small, and it may be affected by the assumptions in our model.

6. Conclusions

Polar-plane-free, faceted InGaN QWs grown on the semipolar $(\bar{1}\bar{1}2\bar{2})$ plane was compared with the 3D QWs on (0001). It was found that inter-facet variation of effective InN thickness is quite different between them. This observation is interpreted as an influence of the crystallographic orientation dependence of the In incorporation efficiency. The inclined $(\bar{1}10\bar{1})$ in the 3D QWs on $(\bar{1}\bar{1}2\bar{2})$ has significantly higher In incorporation efficiency, resulting in the suppression of surface In adatom migration. The weakened In adatom diffusion on the inclined $(\bar{1}10\bar{1})$ is also suggested from both the diffusion equation analyses and the simplified model calculation. Such growth behavior causes the different emission-wavelength distribution between the 3D QWs on (0001) and $(\bar{1}\bar{1}2\bar{2})$.

Acknowledgments

References

[1] K. Nishizuka, M. Funato, Y. Kawakami, Sg. Fujita, Y. Narukawa, and T. Mukai, "Efficient radiative recombination from ⟨11$\bar{2}$2⟩-oriented In$_x$Ga$_{1-x}$N multiple quantum wells fabricated by the regrowth technique," Appl. Phys. Lett., vol.85, no.15, pp.3122–3124, Oct. 2004.

[2] M. Funato, T. Kotani, T. Kondou, Y. Kawakami, Y. Narukawa, and T. Mukai, "Tailored emission color synthesis using microfacet quantum wells consisting of nitride semiconductors without phosphors," Appl. Phys. Lett., vol.88, pp.261920–261923, June 2006.

[3] S.-H. Lim, Y.-H. Ko, C. Rodriguez, S.-H. Gong, and Y.-H. Cho, "Electrically driven, phosphor-free, white light-emitting diodes using gallium nitride-based double concentric truncated pyramid structures," Light: Sci. Appl., vol.5, pp.e16030-e16036, Feb. 2016.

[4] T. Wunderer, J. Wang, F. Lipski, S. Schwaiger, A. Chuvilin, U. Kaiser, S. Metzner, F. Bertram, J. Christen, S.S. Shirokov, A.E. Yunovich, and F. Scholz, "Semipolar GaInN/GaN light-emitting diodes grown on honeycomb patterned substrates," Phys. Status Solidi C, vol.7, no.7-8, pp.2140–2143, May 2010.

[5] T. Wunderer, M. Feneberg, F. Lispki, J. Wang, R.A.R. Leute, S. Schwaiger, K. Thonke, A. Chuvilin, U. Kaiser, S. Metzner, F. Bertram, J. Christen, G.J. Beirne, M. Jetter, P. Michler, L. Schade, C. Vierheilig, U.T. Schwarz, A.D. Dräger, A. Hangleiter, and F. Scholz, "Three-dimensional GaN for semipolar light emitters," Phys. Status Solidi B, vol.248, no.3, pp.549–560, Oct. 2011.

[6] M. Funato, T. Kondou, K. Hayashi, S. Nishiura, M. Ueda, Y. Kawakami, Y. Narukawa, and T. Mukai, "Monolithic polychromatic light-emitting diodes based on InGaN microfacet quantum wells toward tailor-made solid-state lighting," Appl. Phys. Express, vol.1, pp.011106-011109, Jan. 2008.

[7] T. Takeuchi, H. Amano, and I. Akasaki, "Theoretical study of orientation dependence of piezoelectric effects in wurtzite strained GaInN/GaN heterostructures and quantum wells," Jpn. J. Appl. Phys., vol.39, no.2A, pp.413–416, Feb. 2000.

[8] S.-H. Park, "Crystal orientation effects on electronic properties of wurtzite InGaN/GaN quantum wells," J. Appl. Phys., vol.91, no.12, pp.9904–9908, June 2002.

[9] Y. Matsuda, M. Funato, and Y. Kawakami, "Polychromatic emission from polar-plane-free faceted InGaN quantum wells with high radiative recombination probabilities," Appl. Phys. Express, vol.10, pp.071003-071006, June 2017.

[10] M. Ueda, K. Hayashi, T. Kondou, M. Funato, Y. Kawakami, Y. Narukawa, and T. Mukai, "Mechanisms of metalorganic vapor phase epitaxy of InGaN quantum wells on GaN microfacet structures," Phys. Status Solidi C, vol.4, no.7, pp.2826–2829, May 2007.

[11] T. Wernicke, L. Schade, C. Netzel, J. Rass, V. Hoffmann, S. Ploch, A. Knauer, M. Weyers, U. Schwarz, and M. Kneissl, "Indium incorporation and emission wavelength of polar, nonpolar and semipolar InGaN quantum wells," Semicond. Sci. Technol., vol.27, pp.024014-024020, Jan. 2012.

[12] Y. Wang, R. Shimma, T. Yamamoto, H. Hayashi, K.-I. Shiohama, K. Kurihara, R. Hasegawa, and K. Ohkawa, "The effect of plane orientation on indium incorporation into InGaN/GaN quantum wells fabricated by MOVPE," J. Cryst. Growth, vol.416, pp.164–168, April 2015.

[13] R. Bhat and G.M. Guryanov, "Experimental study of the orientation dependence of indium incorporation in GaInN," J. Cryst. Growth, vol.433, pp.7–12, Jan. 2016.

Yoshinobu Matsuda is a Ph.D student of Electronic Science and Engineering, Kyoto University. He received the B.S. and M.S. degrees in Electronic Science and Engineering, Kyoto University, Kyoto, Japan, in 2015, and 2017, respectively.

Mitsuru Funato is an associate professor of Electronic Science and Engineering, Kyoto University. He received the B.S., M.S., and D.S. degrees from Kyoto University, Kyoto, Japan, in 1989, 1991, and 1998, respectively. Since 1991, he was a research associate in the Department of Electrical Engineering, Kyoto University, where he became an lecture in 2002, and was promoted to an associate professor in the Department of Electronic Science and Engineering in 2007. During 2000–2001, he was a visiting research fellow in the Department of Physics, Heriot-Watt University, U.K. His current research interests include crystal growth, characterization, and device applications of nitride semiconductors.

Yoichi Kawakami is a professor of Electronic Science and Engineering, Kyoto University. He revived the B.S., M.S., and D.S. degrees in electrical engineering from Osaka University, Osaka, Japan, in 1984, 1986, and 1989, respectively. He was a research associate in the Department of Electrical Engineering, Kyoto University, Kyoto, Japan, where he became an associate professor in 1997, and was promoted to a professor in the Department of Electronic Science and Engineering in 2007, and was engaged in research on II-VI widegap semiconductors. During 1991–1992, he was a visiting research fellow in the Department of Physics, Heriot-Watt University, U.K. He was awarded the JSAP fellow from The Japan Society of Applied Physics in 2011. His current research interests include spatial and temporal luminescence spectroscopy of excitons in GaN-based low-dimensional semiconductors, fabrication of new photonic devices, as well as application of solid-state lighting using white light-emitting diodes.